Biophysical Journal Volume 109 November 2015 1925–1936

Article

Plasma Membrane Organization of Epidermal Growth Factor Receptor in Resting and Ligand-Bound States

Nirmalya Bag,[1] Shuangru Huang,[1] and Thorsten Wohland[2,*]

[1]Department of Biological Sciences and Centre for Bioimaging Sciences; and [2]Department of Chemistry, National University of Singapore, Singapore

ABSTRACT The spatial arrangement of the epidermal growth factor receptor (EGFR) on the cellular plasma membrane is one of the prime factors that control its downstream signaling pathways and related functions. However, the molecular organization, which spans the scale from nanometers to micrometer-size clusters, has not been resolved in detail, mainly due to a lack of techniques with the required spatiotemporal resolution. Therefore, we used imaging total internal reflection-fluorescence correlation spectroscopy to investigate EGFR dynamics on live CHO-K1 plasma membranes in resting and ligand-bound states. In combination with the fluorescence correlation spectroscopy diffusion law, this provides information on the subresolution organization of EGFR on cell membranes. We found that overall EGFR organization is sensitive to both cholesterol and the actin cytoskeleton. EGFR in the resting state is partly trapped in cholesterol-containing domains, whereas another fraction exhibits cholesterol independent trapping on the membrane. Disruption of the cytoskeleton leads to a broader range of EGFR diffusion coefficients and a reduction of hop diffusion. In the ligand-bound state we found a dose-dependent behavior. At 10 ng/mL EGF the EGFR is endocytosed and recycled to the membrane, whereas diffusion and organization do not change significantly. At 100 ng/mL EGF the EGFR forms clusters, which are subsequently internalized, whereas outside the clusters diffusivity increases and the organization of the receptor remains unchanged. After disruption of cholesterol-containing domains or actin cytoskeleton, EGF induces microscopic EGFR clusters on the membrane and endocytosis is inhibited.

INTRODUCTION

Epidermal growth factor receptor (EGFR) is a prototypical receptor tyrosine kinase that belongs to the ErbB family. It is a key regulator of a variety of physiological processes ranging from cell proliferation to apoptosis (1). EGFR activation leads to signal transduction and initiation of various downstream signaling cascades (2). It is believed that EGFR is inhomogeneously distributed on the membrane and its oligomeric state, on which its functions strongly depend, is majorly dictated by this organization and concomitant dynamics (3,4). It was recently shown, by combination of experiments and molecular dynamics simulations, that the interaction of EGFR with the surrounding lipid bilayer on plasma membranes plays a fundamental role in the formation of active dimers after ligand binding (5,6). However, the membrane organization of EGFR and its relationship to the ligand-induced clustering, phosphorylation, and endocytosis are controversial (7–9). This is mainly due to the complex organization of plasma membranes, exhibiting patterns on a wide range of spatial and temporal scales (10). Nevertheless, EGFR oligomerization pre- and postligand stimulation is linked with its lateral dynamics and organization on the plasma membrane, which in turn has a strong effect on EGFR signaling (11–13).

According to the classical description of the plasma membrane organization, a variety of ordered domains with distinct physicochemical properties are embedded within the phospholipid bilayer matrix. These domains, depending on their composition, are generally categorized as cholesterol- and sphingolipid-enriched lipid rafts, cholesterol and glycolipid-containing caveolae, and cholesterol-deficient domains such as ganglioside domains. Membrane proteins are often found to have a preferred localization in these domains. Glycosylphosphatidylinositol anchored proteins (GPI-APs) and caveolin-1 are found in lipid rafts and caveolae, respectively (14,15). Membrane domains, in the resting cells, are believed to be randomly distributed over the entire membrane and act as transient trapping sites of localized biomolecules (16). In parallel, the actin cytoskeleton meshwork creates a spatial pattern underneath the membrane that can influence the membrane organization. Transmembrane proteins are often immobilized at the mesh boundary (17). The mesh boundary along with the immobilized proteins poses a barrier against free diffusion across the membrane plane. Transient trapping in membrane domains and diffusion barriers formed by the cytoskeleton meshwork result in non-Brownian membrane diffusion (18). This unique architecture of membranes plays a pivotal role in biological functions, including the oligomerization state of membrane

Submitted July 6, 2015, and accepted for publication September 8, 2015.

*Correspondence: twohland@nus.edu.sg

Nirmalya Bag and Shuangru Huang contributed equally to this work.

Editor: Kalina Hristova.

0006-3495/15/11/1925/12

http://dx.doi.org/10.1016/j.bpj.2015.09.007

proteins, signal transduction, endocytosis, and cell-cell communication (19).

Here, we quantitate the lateral diffusion and organization of EGFR in resting and ligand-bound states on live CHO-K1 plasma membranes at physiological conditions by imaging total internal reflection-fluorescence correlation spectroscopy (ITIR-FCS) where the membrane-bound fluorophores are excited with TIR illumination and the fluorescence signal is collected by a fast and sensitive camera (20). ITIR-FCS breaks the single spot limitation of conventional FCS by performing FCS experiments on thousands of contiguous spots in parallel and provides diffusion coefficient (D) maps of a sample. However, ITIR-FCS is a diffraction-limited technique, whereas the receptor spatial heterogeneity is on the nanometer scale. To address this limitation, we adopted the FCS diffusion law (21) for ITIR-FCS. The dependence of the diffusion time of a probe molecule ($\tau_D = A_{eff}/D$) on the size of the observation area (A_{eff}) gives rise to the FCS diffusion law plot (Eq. S2 in the Supporting Material). This plot, when extrapolated to zero, yields the FCS diffusion law intercept (τ_0), which provides information on the spatial organization of the probe below the diffraction limit. The value of τ_0 is zero for free diffusion, positive for transient confinement in domains, and negative for hop diffusion due to a meshwork (21,22). Note that both transient molecular trapping in lipid domains and assembly of proteins to form transient clusters followed by disassembly give rise to positive intercept in the FCS diffusion law plot. In the first case, the trapping time of the probe molecule is smaller than the lifetime of the domains. In contrast, the trapping time and domain lifetime are the same in the second case. The FCS diffusion law can be easily implemented in ITIR-FCS, as observation areas of different size can be created by pixel binning of the recorded image stack. Thus, ITIR-FCS in combination with the FCS diffusion law extracts subresolution information of living systems from diffraction-limited measurements and thus is an ideal choice to observe nanoscale spatiotemporal organization of membrane receptors.

We first performed proof-of-principle experiments on DiI-C_{18}, green fluorescent protein (GFP)-GPI-AP, and a GFP fused to a plasma membrane targeting sequence (PMT-GFP) on CHO-K1 cells to confirm that they undergo free diffusion, cholesterol-dependent domain confined diffusion, and actin-dependent hop diffusion, respectively. The dynamics and organization of EGFR-EGFP is found to be more complex. In the resting state, the receptor is spatially confined on the cell membrane in a cholesterol and cortical actin dependent manner. Moreover, a significant amount of cholesterol-independent trapping of EGFR-EGFP diffusion was also observed. This either could originate from dynamic partitioning of EGFR in the cholesterol-independent domains or by the formation of receptor clusters. The organizational features change significantly when EGFR is stimulated with its cognate ligand, epidermal growth factor (EGF). The diffusivity, clustering, and internalization of EGFR are dependent on ligand dose. We further observed that the internalization of the ligand-bound EGFR is compromised in the absence of cholesterol-dependent domains or after actin cytoskeleton disruption, both of which allow EGFR clusters to stay on the membrane for a longer time.

MATERIALS AND METHODS

Protocols for the preparation of lipid bilayers, cell culture, transfection, chemical labeling, and drug treatment are provided in detail in the Supporting Material. The imaging setup, data acquisition, and analysis procedures are reported elsewhere (23–26) and also given briefly in the Supporting Material.

RESULTS AND DISCUSSION

ITIR-FCS was employed to quantify the distribution of the lateral diffusion coefficient (D) of EGFR-EGFP, whereas FCS diffusion law analysis was performed on the same set of data to understand its spatial heterogeneity in terms of transient trapping inside membrane domains or clustering and compartmentalization due to the actin network. The FCS diffusion law intercept (τ_0) quantitatively describes obstructed diffusion in these cases. The τ_0 is positive for transient trapping or clustering and negative for meshwork compartmentalization. The magnitude of τ_0 for domain confinement increases with confinement size, confinement time, and partitioning into the domains. The value of τ_0 for hop diffusion across a meshwork depends on the size and density of the mesh and the hopping frequency of the probe molecules. The change of membrane diffusion and confinement of EGFR-EGFP is compared to those of a well-established lipid raft marker, GFP-GPI-AP, and freely diffusing probe, DiI-C_{18}, after cholesterol depletion or actin depolymerization. By connecting these observations, we construct the spatial arrangement of EGFR on the plasma membrane and also address individual contributions from each of the organizational elements. We further explore how this organization in the resting state is modified after stimulation with high and low doses of EGF. Imaging of ligand-induced EGFR endocytosis and microscopic clustering corroborates the cell surface organization, deduced from the FCS diffusion law analysis.

EGFP was fused at the C-terminus of EGFR. The plasmid map has been previously published (27). Methyl beta cyclodextrin (mβCD) and Latrunculin A (Lat A) were used to modify membrane organization by disrupting cholesterol-containing rafts and caveolae (28) and actin cytoskeleton depolymerization (29), respectively. All measurements were conducted on live CHO-K1 plasma membranes at 37°C and 5% CO_2 environment unless mentioned otherwise. Cells expressing EGFR were starved by incubation in serum-free medium for 4 h before measurements. All ITIR-FCS measurements were taken with a recording time of 1 ms (for DiI-C_{18}) or 2 ms (for GFP-GPI-AP and

EGFR-EGFP) per frame. Note that photodynamic processes and cytosolic diffusion of EGFR-EGFP are expected to have characteristic times below 1 ms (30–32). They are therefore unlikely to interfere in the quantification of the membrane diffusion of EGFR-EGFP. We first demonstrate the applicability of the FCS diffusion law to determine the organization of live CHO-K1 cells and various model membranes. The principle of the FCS diffusion law is provided in the Supporting Material.

The ITIR-FCS diffusion law describes organization of lipids and proteins

We used three different membrane probes, namely DiI-C_{18}, GFP-GPI-AP, and PMT-GFP, and determined their diffusion and confinement modes on plasma membranes (Fig. 1). The total internal reflection fluorescence (TIRF) images of the cells labeled with the previous probes were optically homogeneous (Fig. 1, *images*). The D of DiI-C_{18} and GFP-GPI-AP was 1.34 $\pm$ 0.20 $\mu m^2/s$ and 0.31 $\pm$ 0.22 $\mu m^2/s$, respectively, at 37°C (see Fig. S8, *blue* and *black*). A similar difference between DiI-C_{18} and GFP-GPI-AP diffusion was reported for RBL and HeLa cells (24,33).

The FCS diffusion law analyses also showed a clear difference in the subresolution membrane heterogeneity mirrored by DiI-C_{18} and GFP-GPI-AP diffusion. The τ_0 of DiI-C_{18} and GFP-GPI-AP was -0.05 ± 0.01 s and 1.27 ± 0.05 s, respectively (Fig. 1, *bottom*). Note that the margin of error for the ITIR-FCS diffusion law intercept is $\pm$ 0.1 s and thus values of τ_0 in that range are consistent with free diffusion (25). After mβCD treatment, τ_0 of GFP-GPI-AP was reduced to 0.17 $\pm$ 0.11 s, whereas D increased to 0.44 $\pm$ 0.22 $\mu m^2/s$. This confirms free diffusion for DiI-C_{18} and cholesterol-dependent domain confinement for GFP-GPI-AP (34). PMT-GFP was shown to be located in the inner leaflet of the plasma membrane and was associated with the actin cytoskeleton in CHO-K1 and macrophages cells (35,36). The values of D and τ_0 of PMT-GFP were 0.67 $\pm$ 0.20 $\mu m^2/s$ and -0.63 ± 0.02 s, respectively (Fig. 1, *bottom*), suggesting hop diffusion. When the actin cytoskeleton was disrupted, τ_0 increased to 0.06 $\pm$ 0.02 s, indicating free diffusion. However, D (after treatment: 0.62 $\pm$ 0.22 $\mu m^2/s$) did not change significantly. Thus, the diffusion of PMT-GFP is spatially compartmentalized by the actin cytoskeleton meshwork. These results in live cell membranes establish the potential of the ITIR-FCS diffusion law to elucidate subresolution localization of probe molecules (see Fig. S1 for similar measurements on lipid bilayers).

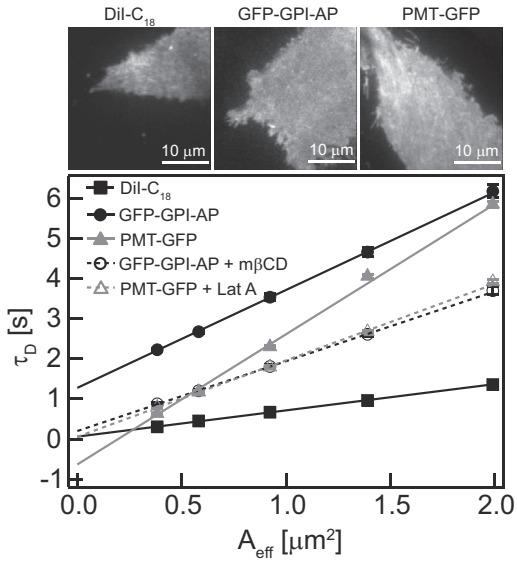

FIGURE 1 Demonstration of ITIR-FCS diffusion law on live cell membranes expressing different proteins or stained with lipid probes that exhibit various modes of diffusion.

Spatiotemporal diffusion and organization of EGFR on the plasma membranes in the resting state

EGFR trapping on the plasma membranes is partially dependent on cholesterol

The values of D of EGFR-EGFP were 0.20 $\pm$ 0.13 $\mu m^2/s$ at 37°C, which is slower than that of GFP-GPI-AP (0.31 $\pm$ 0.22 $\mu m^2/s$) (Fig. S1, *red* and *black*). In addition, the τ_0 values of EGFR-EGFP (1.5–2.5 s) were always larger than that of GFP-GPI-AP (1.0–1.3 s). Therefore, overall domain confinement of EGFR-EGFP is stronger than that of GFP-GPI-AP. We first probe the contribution of cholesterol-containing domains (lipid rafts and caveolae) to achieve such strong confinement. Cells were incubated with 3 mM mβCD and D and τ_0 of EGFR were monitored for up to 1 h. 3 mM mβCD is sufficient to deplete cholesterol-containing domains (37,38). Since in the ITIR-FCS diffusion law, multiple observation areas are measured in a single FCS experiment, one can monitor the time evolution of spatial heterogeneity of a tracer on the membrane under perturbing conditions (23,39).

The time-dependent change of D and τ_0 of EGFR-EGFP after mβCD treatment for one representative cell is shown in Fig. 2, *A* and *B*. The value of D increased monotonically ~40% (from 0.20 $\pm$ 0.13 $\mu m^2/s$ to 0.28 $\pm$ 0.17 $\mu m^2/s$) within ~30 min of the mβCD addition and then decreased toward the initial value after ~50 min incubation (D = 0.21 $\pm$ 0.16 $\mu m^2/s$) (Fig. 2, *A* and *B*, *black*). Fig. 2 *C* shows the D distribution of EGFR-EGFP before and 30 min after mβCD treatment. The distribution is created by pooling D values from 5 cells. The data of individual cells is shown in Fig. S9. The increase in overall membrane diffusion is more obvious in the cumulative distribution of D, which was right shifted with an unchanged slope after treatment (Fig. 2 *C*, *inset*). Likewise, EGFR-EGFP organization became less confined as τ_0 monotonically decreased by ~65% from the basal value of 1.98 $\pm$ 0.72 s to the lowest

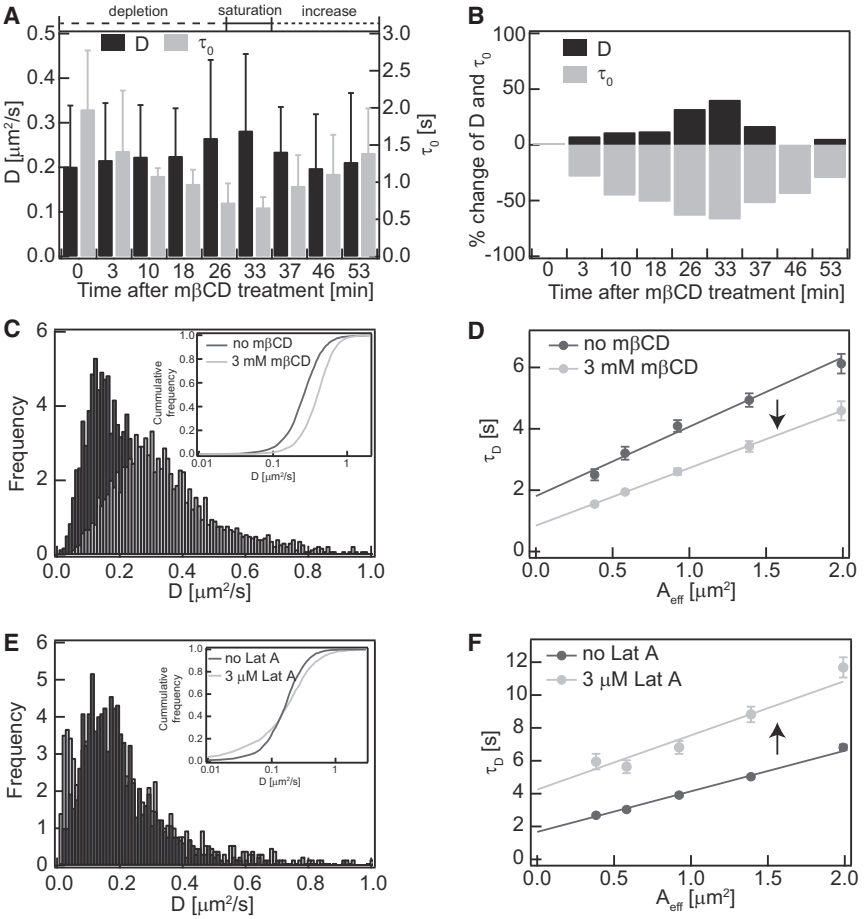

FIGURE 2 Cholesterol and actin cytoskeleton dependence of EGFR localization on CHO-K1 cell membranes. 3 mM mβCD treatment: (*A*) Change of diffusion coefficient (*D*, *black*) and FCS diffusion law intercept (τ_0, *gray*) from one representative cell. We could observe an overall faster diffusion and steady disappearance of membrane heterogeneity until 33 min after treatment (*dashed line*, depletion). This is the time point where mβCD is saturated with the extracted cholesterol (*solid line*, saturation). This is followed by the recovery of membrane heterogeneity (*dotted line*, increase). (*B*) Extent of change of *D* and τ_0 over time. (*C*) Distribution of *D* before and 33 min after treatment (Number of ACFs = 2205 and Number of cells = 5). In the inset, the cumulative distribution of the histograms is shown. (*D*) Representative FCS diffusion law plots for treated and untreated cells. The arrow represents reduction of τ_0. 3 μM Lat A treatment: (*E*) Distribution of *D* before and 15 min after treatment (Number of ACFs = 2205 and Number of cells = 5). In the inset, cumulative distribution of the histograms is shown. (*F*) Representative FCS diffusion law plots for treated and untreated cells. The arrow represents elevation of τ_0.

value of 0.66 $\pm$ 0.14 s at 33 min (Fig. 2, *A*, *B*, and *D*, *gray*). We also observed a similar time-dependent change of GFP-GPI-AP diffusion under identical perturbing conditions (Fig. S2, *A–C*, *black*). However, there is a significant difference in the absolute values. In the case of GFP-GPI-AP, the value of τ_0 is almost zero at ~30 min posttreatment (from 1.31 $\pm$ 0.31 s to 0.17 $\pm$ 0.11 s) indicating free diffusion of GFP-GPI-AP, which is released from lipid rafts after cholesterol extraction (Fig. S2, *A*, *B*, and *D*, *gray*). In contrast, the τ_0 value for EGFR-EGFP decreases but remains strongly positive (0.96 $\pm$ 0.07 s) under the same condition. This suggests only partial cholesterol dependence of EGFR localization and at least some cholesterol independent confinement.

On a side note, we would like to remark that τ_0 for both EGFR-EGFP and GFP-GPI-AP recovered to ~70% of the basal value after prolonged incubation with mβCD (Fig. 2, *A* and *B*, for EGFR and Fig. S2, *A* and *B*, for GPI-AP). In this context, we found that the decrease of τ_0 value depends on the incubation time and concentration of mβCD. The recovery of τ_0 after prolonged duration is due to the saturation of mβCD (Figs. S3 *A* and S4 *A*). Therefore, if longer observation times are required an exchange of the mounting medium with fresh mβCD is required upon mβCD saturation. In addition, this means that the maximum effect of mβCD can be observed only in a relatively narrow time window of ~10 min, at a time point, whose position is dependent on the mβCD concentration.

Therefore, GFP-GPI-AP exclusively partitions into cholesterol-containing domains where a significant amount of EGFR-EGFP also resides. Another fraction of EGFR shows cholesterol-independent trapping. It was earlier suggested that EGFR clusters exist on the membrane in the absence of ligand (40,41), whereas Hofman et al. showed that EGFR resides in cholesterol-independent GM1 domains in the resting state (42). Therefore, the origin of the cholesterol-independent part of τ_0 could be both dynamic formation of EGFR clusters and partitioning into cholesterol-independent domains. Such cholesterol independent trapping of signaling molecules in protein clusters is known for T-cell receptors in the activated state (43). Both *D* and τ_0, as anticipated, remained unaffected for DiI-C_{18}-labeled membranes, confirming that cholesterol extraction does not affect the dynamics of the freely diffusing phospholipid matrix (Fig. S5).

Cholesterol-dependent trapping of EGFR on the plasma membrane is due to its localization in cholesterol-containing domains such as lipid rafts or caveolae. Biochemical studies showed that 40% of EGFR is localized in lipid rafts, whereas

only 5–10% is in caveolae in HEp-2 and A431 cells (44). It was also reported by fluorescence lifetime imaging microscopy-fluorescence resonance energy transfer experiments that EGFR in a resting state colocalizes with GM1, but not with GPI-AP, in HER14 cells (42). The authors found that GPI-AP colocalizes with GM1 in a cholesterol-dependent manner implying that EGFR partitions into cholesterol-deficient GM1 domains. However, the colocalization between caveolae and EGFR was not explored. To test this, we performed experiments on Jurkat T cells that lack caveolae (45). If the cholesterol-dependent fraction of EGFR is exclusively located in caveolae then cholesterol depletion from Jurkat cells would not lead to any change in the EGFR-EGFP confinement, although the same treatment on the GFP-GPI-AP expressing cells would remove its cholesterol-dependent domain confinement. The value of D of EGFR-EGFP in Jurkat cells increased from 0.23 ± 0.16 $\mu m^2/s$ to 0.51 ± 0.39 $\mu m^2/s$ after mβCD treatment (Fig. S10 *A*). An increase in D was also observed for GFP-GPI-AP (before: 0.42 ± 0.23 $\mu m^2/s$ and after: 0.52 ± 0.22 $\mu m^2/s$) (Fig. S10 *C*). For EGFR-EGFP, τ_0 changed from 2.61 ± 0.13 s to 1.17 ± 0.17 s (~56% decrease) (Fig. S10 *B*). Similarly, for GFP-GPI-AP, it was 1.09 ± 0.17 s (before) and 0.28 ± 0.12 s (after) (Fig. S10 D). The relative decrease of τ_0 of EGFR-EGFP after mβCD treatment was also comparable for CHO-K1 (~65%) and Jurkat cells (~56%). Similarly for GFP-GPI-AP, τ_0 decreases to values close to 0.1 s (free diffusion). These observations indicate that the entire cholesterol-dependent fraction of EGFR is located in lipid rafts in the absence of caveolae (Jurkat cells). Therefore, cholesterol-dependent confinement of EGFR in CHO-K1 cells is unlikely to originate from localization in caveolae. This is different from EGFR organization in HER14 cells where it is excluded from lipid rafts in the resting state (42). Thus, localization of EGFR depends on the cell type and availability of various types of cholesterol-containing domains. Nevertheless, a significant fraction of cholesterol-independent confinement of EGFR is common in both CHO-K1 and Jurkat cells, whereas GFP-GPI-AP confinement exclusively depends on cholesterol. Similarly, the degree of confinement (τ_0 value) of EGFR-EGFP is higher than that of GFP-GPI-AP, which is reflected in their respective lateral dynamics, i.e., D of GFP-GPI-AP is larger than that of EGFR-EGFP in resting cells.

EGFR organization depends on actin cytoskeleton

The role of the actin cytoskeleton on EGFR organization was studied next by treating the cells with 3 μM Lat A. Fig. S6 shows images of CHO-K1 cells stably expressing GFP-labeled actin (Lifeact cells) (46) before and after treatment to confirm drug activity. We observed microscopic clusters of EGFR-EGFP in ~20% of cells after the addition of Lat A (Fig. S11 *A*). The average D of EGFR-EGFP, consistent with the literature (47), increased slightly, from 0.20 ± 0.13 $\mu m^2/s$ to 0.26 ± 0.28 $\mu m^2/s$, after actin depolymerization. A closer look at the D distribution shows that the fraction of slow diffusing species ($D < 0.1$ $\mu m^2/s$) increased, whereas that of the fast diffusing species ($D > 0.5$ $\mu m^2/s$) increased slightly after Lat A treatment (Fig. 2 *E*). The species exhibiting intermediate diffusivity ($D = 0.1$–0.5 $\mu m^2/s$) decreased moderately in population. This is more obvious in the cumulative distribution of D (Fig. 2 *E*, *inset*). The population of fast diffusing species increases because the cytoskeleton bound EGFR is released after treatment and they diffuse at a faster rate. On the other hand, EGFR clustering after Lat A treatment results in a slow diffusive fraction. The probability of receptor clustering is dependent on its concentration and the meshwork density (48,49). At low receptor concentration, which is the case here, the cytoskeleton compartments inhibit receptor clustering. However, the receptors are spatially less constrained in the absence of a meshwork and thus the probability of cluster formation increases.

The τ_0 value increased ~55% after cytoskeleton disruption (τ_0 = 1.57 ± 0.11 s to 2.46 ± 0.10 s) (Fig. 2 *E*). This is reminiscent of what was observed for PMT-GFP (Fig. 1 *B*). The reduction and elevation of the τ_0 value after mβCD and Lat A treatment, respectively, confirm the influence of both, membrane domains and cytoskeleton meshwork, on EGFR organization. A similar phenomenon was also observed for other transmembrane proteins such as dipeptidyl peptidase IV (DPP_{IV}-GFP) on live COS-7 cells (38) and NKp46 receptor on hyporesponsive natural killer (NK) cells (50). A negligible effect on D and τ_0 was observed upon the same treatment on either GFP-GPI-AP transfected or DiI-C_{18} stained cells (Fig. S7). Therefore, the membrane organization of GFP-GPI-AP and lipids, in concordance with the previous reports (36,38,51), is not strongly affected by the actin cytoskeleton in live cells.

Our results suggest that EGFR lateral dynamics and organization is dictated by its confinement in membrane domains and compartmentalization by the actin cytoskeleton in the resting state. The cholesterol-dependent domains are mainly lipid rafts with little contribution of caveolae. A cholesterol-independent transient trapping of EGFR is also identified. The source of this trapping could be either cholesterol-deficient lipid domains or EGFR nanoclusters. It was earlier pointed out that EGFR binds to gangliosides, which could potentially be one of the sources of cholesterol-independent trapping of the receptor (52). The domain confinement is the major mediator of EGFR spatial organization on membranes because we observed an overall positive τ_0 value in unperturbed cell membranes.

Spatiotemporal diffusion and organization of EGFR on the plasma membrane in the ligand-bound state

In this section, we focus on the organization of EGFR after stimulation with its extracellular ligand, EGF. It is believed

that EGF binding to EGFR leads to receptor dimerization, which is the first step of receptor activation (48). In addition, large microscopic clusters, which amplify EGFR signaling, are also shown to form after EGF binding (53). Ligand-bound EGFR internalizes via different endocytosis routes depending on the ligand dose (54). The major internalization pathways are clathrin-mediated (CE) and nonclathrin-mediated endocytosis (NCE) at a low and high dose of EGF, respectively, where NCE is reported to attenuate EGFR signaling (54,55). This suggests that ligand binding, activation, and internalization of EGFR are closely coupled with its localization on the membrane (56,57). However, experimental evidence both supports (58,59) and disputes (57,60) that localization of EGFR in membrane domains promotes EGFR signaling. This ambiguity could well stem from the experimental difficulties that arise from the nanoscopic size of the membrane domains or deleterious effects of chemical treatments. Here, we performed time-lapse confocal imaging to monitor ligand-induced EGFR clustering and endocytosis (61,62). In parallel, we employed TIRF imaging and ITIR-FCS in tandem to elucidate the state of EGFR diffusion and organization above and below the resolution limit upon low and high doses of EGF stimulation. We estimated the cell surface density of EGFR-EGFP to be 20,000–200,000 molecules per cell by confocal FCS, which coincides with reported physiological levels (27,63). This covers the range where 10 and 100 ng/mL of EGF represents low and high dose ligand concentrations (Table S1) (54). We finally studied the contribution of cholesterol-dependent domains and the actin cytoskeleton in EGF-induced modulation of EGFR dynamics.

EGFR clustering and endocytosis after EGF stimulation depends on ligand dose

Time lapse confocal imaging showed the formation of a negligible amount of EGFR clusters on the membrane after 10 ng/mL EGF stimulation (Fig. S12 *A*). Moreover, we observed intracellular fluorescence, although the membrane fluorescence did not change significantly. This is probably due to dynamic recycling of the ligand-bound EGFR, as proposed earlier for low dose stimulation (54). The retention of membrane fluorescence was also observed in the TIRF images (Fig. 3 *A*). On the contrary, macroscopic EGFR-EGFP clusters were formed on the plasma membrane after addition of 100 ng/mL EGF (Fig. S12 *B*). These clusters internalized (13–20 min, Fig. S12 *B*) and gradually disappeared over time (20 min onward, Fig. S12 *B*). A significant drop of membrane signal was also observed in the TIRF images (Fig. 3 *B*). The permanent reduction of membrane fluorescence and gradual fading of intracellular fluorescence could be due to the degradation of the internalized EGFR (54). As a control, GFP-GPI-AP expressing and DiI-C_{18} stained cells were incubated with 100 ng/mL of EGF. We did not observe any cluster of GFP-GPI-AP on the membrane as expected (Fig. S13 *A*). Endocytosis of GFP-GPI-AP after EGF treatment was also not observed (Fig. S12 *C*). Overall, EGF binds to EGFR to form clusters on the membrane, which are eventually internalized. The cluster formation is EGF concentration dependent.

Modulation of EGFR membrane diffusion in relation to EGF concentration

We measured the change of membrane diffusion and heterogeneity of the remaining EGFR after EGF stimulation. At a low dose of EGF (10 ng/mL) both D (before: 0.20 ± 0.13 $\mu m^2/s$ and after: 0.21 ± 0.13 $\mu m^2/s$) and τ_0 (before: 1.69 ± 0.12 s and after: 1.64 ± 0.10 s) of EGFR-EGFP remained unchanged (Fig. 4, *A* and *B*, respectively). Thus, low dose stimulation of EGF does not change membrane dynamics and confinement of EGFR while receptor internalization still occurs but probably with receptor recycling.

After 100 ng/mL EGF stimulation, a small but significant time-dependent change of D of EGFR-EGFP was recorded (Fig. 4, *C* and *D*). The average D increased with time by 35% (from 0.20 ± 0.13 $\mu m^2/s$ to 0.27 ± 0.17 $\mu m^2/s$; Kolmogorov-Smirnov (KS) test $p < 0.001$), whereas τ_0 remained unaltered and positive after ~15–20 min stimulation (before: 1.85 ± 0.12 s and after: 1.93 ± 0.08 s) (Fig. 4, *C–F*). The trend of the temporal change of D was similar to that of mβCD treatment while, for τ_0, it significantly differed (Figs. 2 *B* and 4 *D* for mβCD and EGF treatment, respectively). Therefore, as expected, it is not a common mechanism that modifies EGFR-EGFP diffusion on the membrane upon EGF and mβCD treatments, although the average D after these treatments was very similar (0.28 ± 0.17 $\mu m^2/s$ for mβCD and 0.27 ± 0.17 $\mu m^2/s$ for EGF).

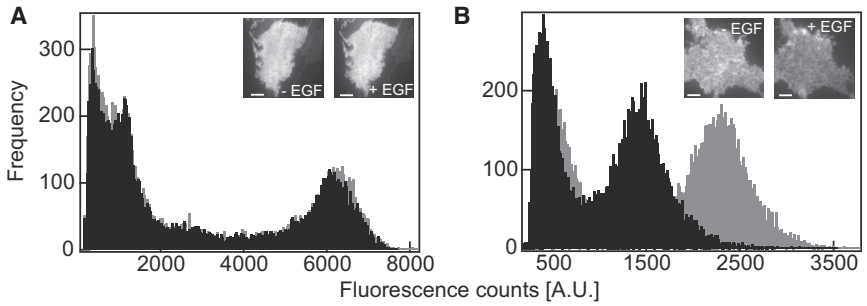

FIGURE 3 Fluorescence intensity histograms and TIRF images of EGFR-EGFP expressing CHO-K1 cells before and 20 min after stimulation with (*A*) 10 ng/mL and (*B*) 100 ng/mL EGF. The fluorescence intensity (before: *gray*; after: *black*) stayed constant at 10 ng/mL but was reduced at 100 ng/ml. The peaks at the extreme left side of both figures are due to electronic background. The scale bar is 5 μm.

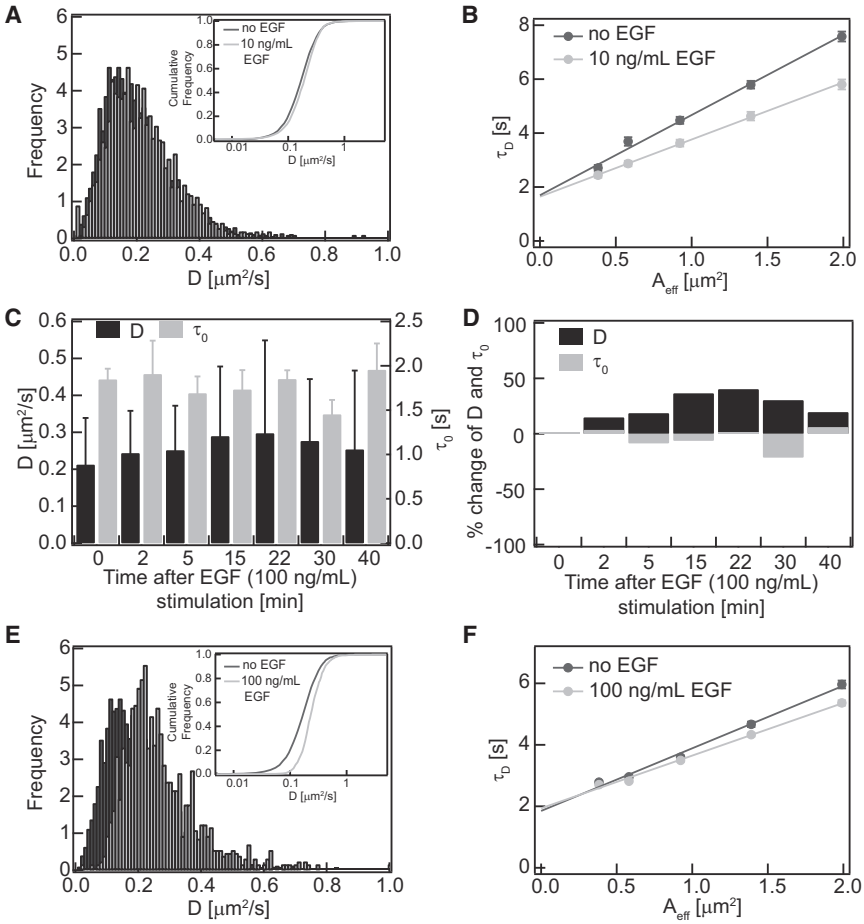

FIGURE 4 Effect of EGF stimulation on the dynamics and organization of EGFR. (*A*) *D* distribution (Number of ACFs = 2205 and Number of cells = 5) and (*B*) FCS diffusion law plot before and 20 min after 10 ng/mL EGF stimulation for one representative cell. (*C*) Change of diffusion coefficient (*D*, black) and FCS diffusion law intercept (τ_0, *gray*) over time after stimulation with 100 ng/mL EGF for one representative cell. (*D*) Extent of change of *D* and τ_0 over time for the same treatment. (*E*) Distribution of *D* before and 20 min after stimulation with 100 ng/mL EGF (Number of ACFs = 2205 and Number of cells = 5). In the inset the cumulative distribution of the histograms is shown. (*F*) Representative FCS diffusion law plots for treated and untreated cells.

An interesting feature can be spotted when the *D* distribution (both histogram and cumulative) of the EGFR after mβCD and EGF treatments is compared. There was a striking drop on the fraction of slow diffusing particles ($D < 0.1$ $\mu m^2/s$) after EGF stimulation in a similar fashion to that after mβCD treatment (Figs. 4 *C* and S14 *A*). However, the fast diffusing fraction in case of EGF stimulation did not increase to the same extent compared to the mβCD treatment. In both cases, the cumulative distribution right shifted from that of the resting state. But the slope of the cumulative plot did not change for mβCD treatment as opposed to the case of EGF stimulation where the slope became steeper (Fig. S14 *B*, *green* versus *black*). Therefore, mβCD causes a global change in EGFR diffusion, whereas the slow diffusing fraction on the membrane surface disappears selectively on EGF stimulation.

The *D* distribution of GFP-GPI-AP did not change after 100 ng/mL EGF addition (before: 0.31 $\pm$ 0.22 $\mu m^2/s$ and after: 0.32 $\pm$ 0.22 $\mu m^2/s$). Similarly, the τ_0 value before (1.15 $\pm$ 0.07 s) and after (1.24 $\pm$ 0.07 s) treatment also shows no prominent change in subresolution domain organization (Fig. S13, *B* and *C*). Similar effects were also observed for DiI-C_{18} diffusion and organization (Fig. S13, *D* and *E*). This confirms that EGF has no influence on GFP-GPI-AP containing cholesterol-dependent domains and the phospholipid-enriched bilayer matrix on resting plasma membranes.

The relationship of EGFR membrane diffusion, confinement, and the mode of internalization in the ligand-bound state

The *D* distribution of EGFR-EGFP following EGF stimulation can be linked to the mode of endocytosis. The major route of receptor internalization is CE. In this mechanism, the receptor is transported via clathrin-coated pits into early endosomes followed by late endosome localization where the fate of the receptor, whether to degrade at the lysosome or to recycle to the membrane, is decided. In contrast, cholesterol-containing domains are involved in NCE. As a result, cholesterol-containing domains disappear from the membrane. Because EGFR is partially localized in cholesterol-dependent domains, NCE of the receptor changes its membrane diffusion. But if cholesterol-dependent domains do not participate in the internalization, as in the case of CE, EGFR diffusion remains unaffected. We also tested NCE by monitoring endocytosis of GFP-GPI-AP and EGFR-mRFP cotransfected cells at a given EGF dose.

The fluorescence signal on the membrane hardly changed after 10 ng/mL EGF stimulation (Fig. 3 *A*). In addition, a

few EGFR clusters on the membrane along with intracellular fluorescence were observed (Fig. S12 *A*). Both membrane and intercellular signal did not vanish after prolonged incubation, nor did the average membrane diffusivity of EGFR change. In the cytosol, we observed fluorescence of EGFR-mRFP but not of GFP-GPI-AP after treatment of 10 ng/mL EGF on the cotransfected cells (Fig. S15 *A*). This implies that GFP-GPI-AP containing cholesterol-dependent domains are not involved in the endocytosis. We therefore rule out the possibility of NCE to be an internalization pathway here. Sigismund et al. reported that the EGFR undergoes CE and is recycled to the membrane after a low dose of ligand stimulation (54). Persistent intracellular fluorescence signal since its first appearance and unchanged membrane fluorescence in our experiments suggests receptor recycling to the membrane after internalization. The D and τ_0 values for EGFR after 10 ng/mL EGF stimulation were unchanged because the trapping sites are not involved in the endocytosis.

After 100 ng/mL EGF addition, we observed both green and red fluorescence in endocytosed clusters of GFP-GPI-AP and EGFR-mRFP cotransfected cells (Fig. S15 *B*). The regions in the cell interior that were devoid of clusters had high amounts of EGFR-mRFP, which did not colocalize with GFP-GPI-AP. The endocytosis of GFP-GPI-AP confirms that the cholesterol-dependent domains are endocytosed and thus it is an NCE process. Note that GFP-GPI-AP itself does not endocytose after EGF treatment in the absence of EGFR (Fig. S12 *C*). In addition, the intracellular EGFR-mRFP signal, which does not colocalize with GFP-GPI-AP suggest a CE process. Interestingly, the average membrane diffusion of the EGFR-EGFP increased (Fig. 4 *E*). This D distribution shows that a slow diffusing ($D < 0.1\ \mu m^2/s$) fraction of EGFR disappeared, whereas the fast diffusing fraction remained unaffected (Fig. 4 *E* and *inset*). The disappearance of the slow diffusing fraction is due to the removal of more ordered and viscous (less fluid) cholesterol-containing domains during NCE. In addition, the fluorescence signal from the membrane did not recover after prolonged incubation, although the internalized clusters that were observed after EGF stimulation (Figs. 3 *B* and S12 *B*) gradually disappeared over time, suggesting degradation of internalized EGFR. This matches well with the literature, which states that ~40% of EGFR is endocytosed via NCE after stimulation with a high dose of EGF and the majority degrades over time (54,64). A recent study shows that the completion of the internalization process takes ~15 min after ligand stimulation (65). This is about the time when we observed the maximum diffusivity of the EGFR on the membranes after EGF stimulation inferring the disappearance of the cholesterol-containing domains to the highest extent (Fig. 4 *D*). Therefore, one of the internalization pathways of EGFR after stimulation with 100 ng/mL EGF is nonclathrin-mediated and cholesterol-dependent endocytosis. Abulrob et al. also reported similar endocytosis and degradation of the domains of intermediate size followed by EGFR recycling to the membrane (66).

An interesting feature in the organization of EGFR-EGFP should be noted here. The τ_0 value did not change after 100 ng/mL EGF stimulation. Therefore, the fraction of membrane area that could trap EGFR remained the same, although cholesterol-containing domains were partially removed during endocytosis. Sergeev et al. reported that the binding of EGF increases the number and size of EGFR clusters (67). EGF also introduces large domains by coalescing various membrane domains (42,68). The existence of these larger nanoclusters/domains would therefore compensate the loss of confinement due to the removal of cholesterol-containing domains and thus result in almost constant τ_0 values. The possibility of formation of macroscopic clusters was tested at a higher concentration of EGF (500 ng/mL). We indeed observed large clusters on the membrane (Fig. S16 *A*) along with endocytosed clusters inside the cells (Fig. S16 *B*).

Overall, the interaction of EGF with membrane-bound EGFR is strongly dependent on EGF concentration. At low dose (10 ng/mL), EGFR internalizes probably via CE with an unchanged membrane diffusion and confinement. At high dose (100 ng/mL), EGFR undergoes both CE and NCE, which leads to a time-dependent increase of its membrane diffusion. In parallel, the remaining EGFR on the membrane assembles into nanoclusters with a larger size and density. The last point was supported by the observation of receptor clustering at even higher dose stimulation (500 ng/mL).

Involvement of cholesterol-dependent domains in EGF-induced EGFR endocytosis

We next investigated the effects of EGF on EGFR organization when the latter is released from cholesterol-dependent domains. The cells were first incubated with 3 mM mβCD for 30 min. At this time point, i.e., when the maximum effect of mβCD in terms of D and τ_0 was observed Fig. 2 *A*), 10 ng/mL of EGF was added to the system. We did not observe any microsocpic clusters on the membrane. Interestingly, the τ_0 value at this condition increased significantly (untreated: 2.14 $\pm$ 0.17 s, mβCD: 1.18 $\pm$ 0.15 s, mβCD + EGF: 3.00 $\pm$ 0.17 s) (Figs. 5 *A* and S17 *A*). This could be due to the existence of nanosclusters (67,69). In contrast, microscopic EGFR clusters were observed on the membrane even after 20 min of 100 ng/mL EGF stimulation on cholesterol-depleted cells (Fig. S17 *C*). These clusters are, in general, randomly distributed over the cell surface, although in some cases they are more populated in the cell periphery (70). This is consistent with the work of Saffarian et al., who reported EGFR clustering on the membrane after cholesterol depletion (71). FCS diffusion law analysis on the membrane regions that were devoid of clusters gave a much larger positive intercept ($\tau_0 = 3.70 \pm 0.19$ s) than

that of the resting membrane ($\tau_0 = 1.89 \pm 0.09$ s) (Figs. 5 *B* and S17 *B*), indicating a larger surface coverage of the nanoscopic clusters compared to the basal state. As a control, serum-starved EGFR-EGFP expressing CHO-K1 cells were incubated with mβCD for 30 min followed by washing out of mβCD with serum-free medium that does not contain EGF. We observed a recovery of τ_0 that does not exceed the basal value for the untreated plasma membrane (Fig. S4 *B*). We, however, did not notice any substantial change in the *D* of EGFR after EGF stimulation (Fig. 5, *A* and *B*).

The internalization of EGFR under cholesterol depletion, as observed by confocal imaging, is impaired for both 10 and 100 ng/mL EGF stimulation (Fig. S18). Pike and Casey also reported a similar observation (60). Overall, EGFR membrane organization and internalization behavior post EGF stimulation strikingly differ in resting (Fig. S12) and cholesterol-depleted CHO-K1 cells (Fig. S18). Cholesterol depletion followed by EGF stimulation thus has two effects: impairment of the internalization of EGFR and stronger confinement of the EGFR on the membranes probably by formation of larger and numerous EGFR clusters.

The actin cytoskeleton promotes internalization of EGFR clusters after EGF stimulation

The role of the actin cytoskeleton in endocytosis was investigated because EGFR is an actin binding protein and its organization is compartmentalized by the actin cytoskeleton (72). To test this, we performed TIRF imaging on EGFR-EGFP expressing cells after 3 μM Lat A treatment for 15 min, followed by EGF stimulation for 20 min. Lat A treatment, as stated earlier, induces clustering of the EGFR-EGFP on the plasma membranes of ~20% of the cells (Fig. S11 *A*). In contrast, ~80% of cells exhibit plasma membrane clustering of EGFR-EGFP when EGF (both 10 and 100 ng/mL) is added to the cytoskeleton depleted cells (Fig. S11, *B* and *C*). We then probed any possible changes in the actin organization during the internalization process. Confocal images of Lifeact cells were taken after EGF stimulation of normal and mβCD-treated cells (Fig. S19). In both cases, we did not observe any microscopic change in cytoskeletal organization. Therefore, involvement of the actin cytoskeleton on ligand-induced EGFR endocytosis and its impairment after cholesterol depletion is not associated with macroscopic actin reorganization. The coordination of cholesterol-containing domains and the cytoskeleton is necessary for EGFR endocytosis after a high dose of EGF stimulation because removal of one of them undermines endocytosis and allows EGFR clusters to remain on the membrane for a prolonged duration. We also tested the role that the actin cytoskeleton plays in the interaction between EGF and GPI-AP. GFP-GPI-AP expressing cells were treated first with 3 μM Lat A for 15 min followed by 100 ng/mL of EGF for 20 min and imaged in TIRF at each step of the treatments. We did not observe any GFP-GPI-AP cluster on the plasma membrane (Fig. S20). This is expected since GFP-GPI-AP was earlier shown to be unaffected by the perturbation of actin organization (Fig. S7). Overall, EGFR clustering (Figs. S17 *C* and S11) on the membrane is mediated by both cholesterol and the cytoskeleton.

CONCLUSIONS

The current ITIR-FCS study investigates the spatial distribution of diffusion of EGFR-EGFP on CHO-K1 plasma membranes via the FCS diffusion law in ITIR-FCS. For this purpose we contrast EGFR dynamics and organization with that of DiI-C_{18} and GFP-GPI-AP. We show, by cholesterol depletion experiments, that GFP-GPI-AP is partitioned into cholesterol-containing domains, whereas DiI-C_{18} is insensitive to cholesterol and exhibits free membrane diffusion. It should be noted here that cholesterol depletion by mβCD from the membrane is strongly dependent on concentration and time of measurement. For instance, 3 and 5 mM mβCD show their maximum effect at very different times (~30 and 15 min after addition, respectively) at which they become saturated. The membrane then gradually restores its heterogeneity presumably from replenishing of cholesterol from internal stores. Therefore, measurements after mβCD treatment have to be performed at a specific time and a narrow time window (~5–10 minutes) to obtain a maximal effect.

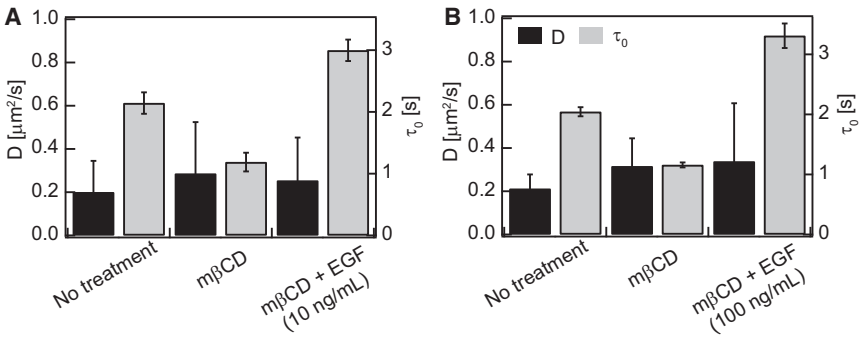

FIGURE 5 Effect of different doses of EGF on the diffusion and heterogeneity of cholesterol depleted EGFR-EGFP expressing CHO-K1 cells. (*A*) 3 mM mβCD for 30 min followed by 10 ng/mL EGF for 20 min, and (*B*) 3 mM mβCD for 30 min followed by 100 ng/mL EGF for 20 min. The τ_0 values after (mβCD + EGF) for both cases are larger than the spontaneous recovered values in case of only mβCD treatment for 50 min (Figs. 1 *A* and S2 *B*). Measurements were done on 3 cells and 1323 ACFs were analyzed at each state of drug treatment.

Our experiments provide evidence of nanoscopic confined diffusion of EGFR in resting cell membranes by cytoskeleton-based compartmentalization and transient trapping in membrane domains. The domain trapping is only partially dependent on cholesterol. Partitioning into cholesterol-independent domains and/or receptor nanoclustering lead to cholesterol-independent trapping of EGFR. Cholesterol-dependent localization of EGFR-EGFP does not require the presence of caveolae. Similar cholesterol dependent and independent trapping is also known for other receptors including T cell and G-protein-coupled receptors (43,73–75). The actin cytoskeleton also plays a significant role in restricting receptors from forming microscopic clusters. EGF, an extracellular ligand of EGFR, modifies the membrane diffusion, clustering, and endocytosis of EGFR-EGFP. Ligand-bound EGFR-EGFP forms clusters that endocytose afterward. The number and size of clusters depends on the ligand dose. Cholesterol-containing domains are involved in the endocytosis only at high dose stimulation, which leads to faster membrane diffusion of the remaining EGFR. The dynamics and organization of GFP-GPI-AP, as expected, does not change upon EGF treatment.

Cholesterol and the actin cytoskeleton play significant roles in the membrane clustering of ligand-bound EGFR. Cholesterol depletion impairs endocytosis of ligand-bound EGFR clusters. This allows the clusters to stay on the membrane for a prolonged duration. This could increase EGFR signaling competency (60,71). Cholesterol-independent EGFR trapping observed here may also play a role in the activation of EGFR after cholesterol depletion. The ligand-bound EGFR clusters on the membrane, regardless of ligand dose, were also observed on actin cytoskeleton-depleted cells. Overall, this study addresses how different membrane organizational principles contribute to EGFR localization and ligand binding on the plasma membranes and also illustrates the link between EGFR endocytosis and modulation of membrane diffusion, confinement, and clustering after EGF binding.

SUPPORTING MATERIAL

Supporting Materials and Methods, Supporting Results, twenty figures, and one table are available at http://www.biophysj.org/biophysj/supplemental/S0006-3495(15)00941-8.

AUTHOR CONTRIBUTIONS

All authors contributed to the experimental design. N.B and S.H. performed experiments. N.B. S.H., and T.W. wrote the article.

ACKNOWLEDGMENTS

The authors acknowledge Dr. Radek Macháň for discussions. John A. Dangerfield, Prof. Alexander Bershadsky, and Prof. Rachel S. Kraut for providing the GFP-GPI-AP construct, Jurkat cells, and Lifeact cells, respectively.

N.B. is supported by the postdoctoral fellowship by a grant from the Ministry of Education Singapore (MOE2012-T3-1-008). S.H. is the recipient of a graduate scholarship of the National University of Singapore. T.W. gratefully acknowledges funding from the Ministry of Education Singapore (MOE2012-T2-1-101).

REFERENCES

1. Normanno, N., A. De Luca, …, D. S. Salomon. 2006. Epidermal growth factor receptor (EGFR) signaling in cancer. *Gene.* 366:2–16.
2. Oda, K., Y. Matsuoka, …, H. Kitano. 2005. A comprehensive pathway map of epidermal growth factor receptor signaling. *Mol. Syst. Biol.* 1:2005.0010.
3. Pike, L. J. 2005. Growth factor receptors, lipid rafts and caveolae: an evolving story. *Biochim. Biophys. Acta.* 1746:260–273.
4. de Laurentiis, A., L. Donovan, and A. Arcaro. 2007. Lipid rafts and caveolae in signaling by growth factor receptors. *Open Biochem. J.* 1:12–32.
5. Endres, N. F., R. Das, …, J. Kuriyan. 2013. Conformational coupling across the plasma membrane in activation of the EGF receptor. *Cell.* 152:543–556.
6. Arkhipov, A., Y. Shan, …, D. E. Shaw. 2013. Architecture and membrane interactions of the EGF receptor. *Cell.* 152:557–569.
7. Valley, C. C., K. A. Lidke, and D. S. Lidke. 2014. The spatiotemporal organization of ErbB receptors: insights from microscopy. *Cold Spring Harb. Perspect. Biol.* 6:a020735.
8. Balbis, A., and B. I. Posner. 2010. Compartmentalization of EGFR in cellular membranes: role of membrane rafts. *J. Cell. Biochem.* 109:1103–1108.
9. Jovin, T. M. 2014. Pinning down the EGF receptor. *Biophys. J.* 107:2486–2488.
10. Nicolson, G. L. 2014. The Fluid-Mosaic Model of Membrane Structure: still relevant to understanding the structure, function and dynamics of biological membranes after more than 40 years. *Biochim. Biophys. Acta.* 1838:1451–1466.
11. Sousa, L. P., I. Lax, …, J. Schlessinger. 2012. Suppression of EGFR endocytosis by dynamin depletion reveals that EGFR signaling occurs primarily at the plasma membrane. *Proc. Natl. Acad. Sci. USA.* 109:4419–4424.
12. Stabley, D., S. Retterer, …, K. Salaita. 2013. Manipulating the lateral diffusion of surface-anchored EGF demonstrates that receptor clustering modulates phosphorylation levels. *Integr. Biol. (Camb.).* 5:659–668.
13. Sawano, A., S. Takayama, …, A. Miyawaki. 2002. Lateral propagation of EGF signaling after local stimulation is dependent on receptor density. *Dev. Cell.* 3:245–257.
14. Simons, K., and J. L. Sampaio. 2011. Membrane organization and lipid rafts. *Cold Spring Harb. Perspect. Biol.* 3:a004697.
15. Escribá, P. V., J. M. González-Ros, …, G. Barceló-Coblijn. 2008. Membranes: a meeting point for lipids, proteins and therapies. *J. Cell. Mol. Med.* 12:829–875.
16. Eggeling, C., C. Ringemann, …, S. W. Hell. 2009. Direct observation of the nanoscale dynamics of membrane lipids in a living cell. *Nature.* 457:1159–1162.
17. Kusumi, A., K. G. Suzuki, …, T. K. Fujiwara. 2011. Hierarchical mesoscale domain organization of the plasma membrane. *Trends Biochem. Sci.* 36:604–615.
18. Krapf, D. 2015. Mechanisms underlying anomalous diffusion in the plasma membrane. *Curr. Top. Membr.* 75:167–207.
19. Lingwood, D., and K. Simons. 2010. Lipid rafts as a membrane-organizing principle. *Science.* 327:46–50.
20. Bag, N., and T. Wohland. 2014. Imaging fluorescence fluctuation spectroscopy: new tools for quantitative bioimaging. *Annu. Rev. Phys. Chem.* 65:225–248.

21. Wawrezinieck, L., H. Rigneault, …, P. F. Lenne. 2005. Fluorescence correlation spectroscopy diffusion laws to probe the submicron cell membrane organization. *Biophys. J.* 89:4029–4042.
22. He, H. T., and D. Marguet. 2011. Detecting nanodomains in living cell membrane by fluorescence correlation spectroscopy. *Annu. Rev. Phys. Chem.* 62:417–436.
23. Bag, N., A. Ali, …, A. Mishra. 2013. Membrane destabilization by monomeric hIAPP observed by imaging fluorescence correlation spectroscopy. *Chem. Commun. (Camb.).* 49:9155–9157.
24. Bag, N., D. H. X. Yap, and T. Wohland. 2014. Temperature dependence of diffusion in model and live cell membranes characterized by imaging fluorescence correlation spectroscopy. *Biochim. Biophys. Acta.* 1838:802–813.
25. Sankaran, J., N. Bag, …, T. Wohland. 2013. Accuracy and precision in camera-based fluorescence correlation spectroscopy measurements. *Anal. Chem.* 85:3948–3954.
26. Guo, S. M., N. Bag, …, M. Bathe. 2014. Bayesian total internal reflection fluorescence correlation spectroscopy reveals hIAPP-induced plasma membrane domain organization in live cells. *Biophys. J.* 106:190–200.
27. Liu, P., T. Sudhaharan, …, T. Wohland. 2007. Investigation of the dimerization of proteins from the epidermal growth factor receptor family by single wavelength fluorescence cross-correlation spectroscopy. *Biophys. J.* 93:684–698.
28. Lajoie, P., and I. R. Nabi. 2010. Lipid rafts, caveolae, and their endocytosis. *Int. Rev. Cell Mol. Biol.* 282:135–163.
29. Yarmola, E. G., T. Somasundaram, …, M. R. Bubb. 2000. Actin-latrunculin A structure and function. Differential modulation of actin-binding protein function by latrunculin A. *J. Biol. Chem.* 275:28120–28127.
30. Sun, G., S. M. Guo, …, T. Wohland. 2015. Bayesian model selection applied to the analysis of fluorescence correlation spectroscopy data of fluorescent proteins in vitro and in vivo. *Anal. Chem.* 87:4326–4333.
31. Widengren, J., U. Mets, and R. Rigler. 1999. Photodynamic properties of green fluorescent proteins investigated by fluorescence correlation spectroscopy. *Chem. Phys.* 250:171–186.
32. Kloster-Landsberg, M., G. Herbomel, …, A. Delon. 2012. Cellular response to heat shock studied by multiconfocal fluorescence correlation spectroscopy. *Biophys. J.* 103:1110–1119.
33. Bacia, K., D. Scherfeld, …, P. Schwille. 2004. Fluorescence correlation spectroscopy relates rafts in model and native membranes. *Biophys. J.* 87:1034–1043.
34. Simons, K., and E. Ikonen. 1997. Functional rafts in cell membranes. *Nature.* 387:569–572.
35. Kapustina, M., T. C. Elston, and K. Jacobson. 2013. Compression and dilation of the membrane-cortex layer generates rapid changes in cell shape. *J. Cell Biol.* 200:95–108.
36. Golebiewska, U., J. G. Kay, …, S. McLaughlin. 2011. Evidence for a fence that impedes the diffusion of phosphatidylinositol 4,5-bisphosphate out of the forming phagosomes of macrophages. *Mol. Biol. Cell.* 22:3498–3507.
37. Mahammad, S., and I. Parmryd. 2008. Cholesterol homeostasis in T cells. Methyl-beta-cyclodextrin treatment results in equal loss of cholesterol from Triton X-100 soluble and insoluble fractions. *Biochim. Biophys. Acta.* 1778:1251–1258.
38. Lenne, P. F., L. Wawrezinieck, …, D. Marguet. 2006. Dynamic molecular confinement in the plasma membrane by microdomains and the cytoskeleton meshwork. *EMBO J.* 25:3245–3256.
39. Huang, H., M. F. Simsek, …, A. Pralle. 2015. Effect of receptor dimerization on membrane lipid raft structure continuously quantified on single cells by camera based fluorescence correlation spectroscopy. *PLoS One.* 10:e0121777.
40. Lemmon, M. A., and J. Schlessinger. 2010. Cell signaling by receptor tyrosine kinases. *Cell.* 141:1117–1134.
41. Yang, S., M. A. Raymond-Stintz, …, B. S. Wilson. 2007. Mapping ErbB receptors on breast cancer cell membranes during signal transduction. *J. Cell Sci.* 120:2763–2773.
42. Hofman, E. G., M. O. Ruonala, …, P. M. van Bergen En Henegouwen. 2008. EGF induces coalescence of different lipid rafts. *J. Cell Sci.* 121:2519–2528.
43. Douglass, A. D., and R. D. Vale. 2005. Single-molecule microscopy reveals plasma membrane microdomains created by protein-protein networks that exclude or trap signaling molecules in T cells. *Cell.* 121:937–950.
44. Ringerike, T., F. D. Blystad, …, E. Stang. 2002. Cholesterol is important in control of EGF receptor kinase activity but EGF receptors are not concentrated in caveolae. *J. Cell Sci.* 115:1331–1340.
45. Orlandi, P. A., and P. H. Fishman. 1998. Filipin-dependent inhibition of cholera toxin: evidence for toxin internalization and activation through caveolae-like domains. *J. Cell Biol.* 141:905–915.
46. Riedl, J., A. H. Crevenna, …, R. Wedlich-Soldner. 2008. Lifeact: a versatile marker to visualize F-actin. *Nat. Methods.* 5:605–607.
47. Boggara, M., K. Athmakuri, …, R. S. Kane. 2013. Characterization of the diffusion of epidermal growth factor receptor clusters by single particle tracking. *Biochim. Biophys. Acta.* 1828:419–426.
48. Grecco, H. E., M. Schmick, and P. I. Bastiaens. 2011. Signaling from the living plasma membrane. *Cell.* 144:897–909.
49. Costa, M. N., K. Radhakrishnan, and J. S. Edwards. 2011. Monte Carlo simulations of plasma membrane corral-induced EGFR clustering. *J. Biotechnol.* 151:261–270.
50. Guia, S., B. N. Jaeger, …, S. Ugolini. 2011. Confinement of activating receptors at the plasma membrane controls natural killer cell tolerance. *Sci. Signal.* 4:ra21.
51. Lebreton, S., S. Paladino, and C. Zurzolo. 2008. Selective roles for cholesterol and actin in compartmentalization of different proteins in the Golgi and plasma membrane of polarized cells. *J. Biol. Chem.* 283:29545–29553.
52. Kawashima, N., S. J. Yoon, …, K. Nakayama. 2009. Tyrosine kinase activity of epidermal growth factor receptor is regulated by GM3 binding through carbohydrate to carbohydrate interactions. *J. Biol. Chem.* 284:6147–6155.
53. Ichinose, J., M. Murata, …, Y. Sako. 2004. EGF signalling amplification induced by dynamic clustering of EGFR. *Biochem. Biophys. Res. Commun.* 324:1143–1149.
54. Sigismund, S., E. Argenzio, …, P. P. Di Fiore. 2008. Clathrin-mediated internalization is essential for sustained EGFR signaling but dispensable for degradation. *Dev. Cell.* 15:209–219.
55. Sorkin, A., and C. M. Waters. 1993. Endocytosis of growth factor receptors. *BioEssays.* 15:375–382.
56. Mayawala, K., D. G. Vlachos, and J. S. Edwards. 2005. Heterogeneities in EGF receptor density at the cell surface can lead to concave up scatchard plot of EGF binding. *FEBS Lett.* 579:3043–3047.
57. Roepstorff, K., P. Thomsen, …, B. van Deurs. 2002. Sequestration of epidermal growth factor receptors in non-caveolar lipid rafts inhibits ligand binding. *J. Biol. Chem.* 277:18954–18960.
58. Balbis, A., A. Parmar, …, B. I. Posner. 2007. Compartmentalization of signaling-competent epidermal growth factor receptors in endosomes. *Endocrinology.* 148:2944–2954.
59. Wang, Y., B. I. Posner, and A. Balbis. 2009. Compartmentalization of epidermal growth factor receptor in liver plasma membrane. *J. Cell. Biochem.* 107:96–103.
60. Pike, L. J., and L. Casey. 2002. Cholesterol levels modulate EGF receptor-mediated signaling by altering receptor function and trafficking. *Biochemistry.* 41:10315–10322.
61. Roepstorff, K., M. V. Grandal, …, B. van Deurs. 2009. Differential effects of EGFR ligands on endocytic sorting of the receptor. *Traffic.* 10:1115–1127.
62. Hofman, E. G., A. N. Bader, …, P. M. van Bergen en Henegouwen. 2010. Ligand-induced EGF receptor oligomerization is kinase-dependent and enhances internalization. *J. Biol. Chem.* 285:39481–39489.
63. Clayton, A. H., F. Walker, …, A. W. Burgess. 2005. Ligand-induced dimer-tetramer transition during the activation of the cell surface

epidermal growth factor receptor-A multidimensional microscopy analysis. *J. Biol. Chem.* 280:30392–30399.

64. Parton, R. G., and K. Simons. 2007. The multiple faces of caveolae. *Nat. Rev. Mol. Cell Biol.* 8:185–194.

65. Villaseñor, R., H. Nonaka, …, M. Zerial. 2015. Regulation of EGFR signal transduction by analogue-to-digital conversion in endosomes. *eLife.* 4:06156.

66. Abulrob, A., Z. Lu, …, L. J. Johnston. 2010. Nanoscale imaging of epidermal growth factor receptor clustering: effects of inhibitors. *J. Biol. Chem.* 285:3145–3156.

67. Sergeev, M., J. L. Swift, …, P. W. Wiseman. 2012. Ligand-induced clustering of EGF receptors: a quantitative study by fluorescence image moment analysis. *Biophys. Chem.* 161:50–53.

68. Hofman, E. G., A. N. Bader, …, P. M. van Bergen En Henegouwen. 2009. EGF induces rapid reorganization of plasma membrane microdomains. *Commun. Integr. Biol.* 2:213–214.

69. Ariotti, N., H. Liang, …, S. J. Plowman. 2010. Epidermal growth factor receptor activation remodels the plasma membrane lipid environment to induce nanocluster formation. *Mol. Cell. Biol.* 30:3795–3804.

70. Winckler, P., L. Lartigue, …, L. Cognet. 2013. Identification and super-resolution imaging of ligand-activated receptor dimers in live cells. *Sci. Rep.* 3:2387–2391.

71. Saffarian, S., Y. Li, …, L. J. Pike. 2007. Oligomerization of the EGF receptor investigated by live cell fluorescence intensity distribution analysis. *Biophys. J.* 93:1021–1031.

72. van Bergen en Henegouwen, P. M. P., J. C. den Hartigh, …, J. Boonstra. 1992. The epidermal growth factor receptor is associated with actin filaments. *Exp. Cell Res.* 199:90–97.

73. Dinic, J., A. Riehl, …, I. Parmryd. 2015. The T cell receptor resides in ordered plasma membrane nanodomains that aggregate upon patching of the receptor. *Sci. Rep.* 5:10082–10090.

74. Chini, B., and M. Parenti. 2004. G-protein coupled receptors in lipid rafts and caveolae: how, when and why do they go there? *J. Mol. Endocrinol.* 32:325–338.

75. Lillemeier, B. F., M. A. Mörtelmaier, …, M. M. Davis. 2010. TCR and Lat are expressed on separate protein islands on T cell membranes and concatenate during activation. *Nat. Immunol.* 11:90–96.